Yes Associated Transcriptional Regulator 1 (YAP1) and WW Domain Containing Transcription Regulator (WWTR1) are required for murine pregnancy initiation

Genna E. Moldovan[1,2], Noura Massri[1,2], Erin Vegter[1], Ivonne L Pauneto-Delgado[3], Gregory W. Burns[2], Niraj Joshi[4], Bin Gu[1,5], Ripla Arora[1,5], Asgerally T. Fazleabas[1,*]

[1]Department of Obstetrics, Gynecology & Reproductive Biology, College of Human Medicine, Michigan State University, Grand Rapids, MI 49503

[2]Cell and Molecular Biology Program, College of Natural Sciences, Michigan State University, East Lansing, MI 48824

[3]University of Puerto Rico Humacao, Humacao, PR 00791

[4]Charles River Laboratories, Mattawan, MI 49071

[5]Institute for Quantitative Health Science and Engineering, Michigan State University, East Lansing, MI 48824

*Corresponding author

Abstract

Endometrial stromal cell decidualization is required for pregnancy success. Although this process is integral to fertility, many of the intricate molecular mechanisms contributing to decidualization remain undefined. One pathway that has been implicated in endometrial stromal cell decidualization in humans *in vitro*, is the Hippo signaling pathway. Two previously conducted studies showed that the effectors of the Hippo signaling pathway, YAP1 and WWTR1, were required for decidualization of primary stromal cells in culture. To investigate the *in vivo* role of YAP1 and WWTR1 in decidualization and pregnancy initiation, we generated a *Progesterone Cre* mediated partial double knockout (pdKO) of *Yap1* and *Wwtr1*. Female pdKOs exhibited subfertility, a compromised decidualization response, partial interruption in embryo transport, blunted endometrial receptivity, delayed implantation and subsequent embryonic development, and a unique transcriptional profile. Bulk mRNA sequencing revealed aberrant maternal remodeling evidenced by significant alterations in extracellular matrix proteins at 7.5 days post coitus in pdKO dams, and enrichment for terms associated with fertility compromising diseases like pre-eclampsia and endometriosis. Our results indicate a required role for YAP1 and WWTR1 for successful mammalian uterine function and pregnancy success.

47

Introduction

Successful reproduction is an impeccably complex process. The coordination of intricate molecular signals with large scale physiological changes imparts many opportunities for error. An unfortunate statistic is that 20% of couples attempting to reproduce are infertile from either male or female contributions (NICHD). Within mammals, the fertilization of ovulated oocyte(s) is just the beginning assuming that ovulation itself is not compromised. Following fertilization and early embryonic development, an embryo implants into a receptive maternal endometrium that is significantly remodeled throughout pregnancy to support gestation(1). In humans and mice, successful reproduction requires the coordinated efforts of many molecular and cellular signals and appropriate interplay between systems including the neuroendocrine, immune, vascular, and female reproductive tract. Humans undergo spontaneous endometrial stromal cell decidualization, a terminal differentiation of the underlying stroma within the endometrium, which is induced by increasing levels of progesterone during the secretory phase of the menstrual cycle(1). This process is critical to control trophoblast invasion and allow appropriate embryo invasion and occurs spontaneously each cycle in the absence of a conceptus(2, 3). In mice, decidualization only occurs when an embryo physically attaches to the maternal endometrial epithelium that communicates with the stroma and initiates decidualization(4). Decidualization both prepares the endometrium for and controls implantation, and the two events are integral in both mice and humans. Therefore, understanding the molecular mechanisms that underly these complex coordinated events is essential to identify mechanisms that may go awry and contribute to infertility.

Many molecular pathways have been implicated in decidualization and implantation including WNT, NOTCH, and HIPPO signaling(5). Of particular interest is the mechanosensing HIPPO pathway. This pathway was first identified in *Drosophila* and so named due to mutations in this pathway leading to increased size(6). The Hippo signaling pathway in mammals controls organ size, growth and proliferation and does so by sensing and responding to changes in the extracellular environment like the presence and tension of nearby cells as well as growth factor availability(7). The Hippo pathway is a kinase cascade whereby external signals like those mentioned above induce the phosphorylation of MST1/2 through a variety of upstream signals. MST1/2 phosphorylate LATS1/2 that then phosphorylate YAP1 and WWTR1, two transcriptional cofactors. When the HIPPO signaling pathway is activated, YAP1 and WWTR1 are inactive in the cytoplasm bound or degraded. Conversely, when the HIPPO signaling pathway is deactivated, YAP1 and WWTR1 translocate to the nucleus and bind their canonical partner transcription factors, the TEADs, where they regulate gene transcription of extracellular and cytoplasmic matrix components, cell cycle genes, and act as distal enhancer recruiters(7). This pathway is well conserved among mammals and has been implicated to play a role in female reproductive function.

Principally, in the murine uterus, YAP1 exhibits dynamic expression with the highest levels of mRNA and protein expression at estrus and diestrus, two estrogen dominated stages (8). Indeed, YAP1 is significantly increased and phosphorylated with 17β-estradiol treatment of ovariectomized mice, suggesting its importance in specific phases

of the estrus cycle(8). Beyond the estrus cycle, YAP1 is expressed throughout the murine endometrium in early pregnancy prior to embryo implantation at embryonic day 0.5 and beyond(9). Post-implantation YAP and its targets, *Ctgf* and *Ankrd1*, are significantly increased. A similar response is observed in oil induced decidualization suggesting a potential role for YAP in maternal preparation of pregnancy(9). In addition, conditional deletion of *Yap1* and its homolog, *Wwtr1*, under *Anti-Mullerian hormone receptor type 2* driven *Cre* expression, results in degradation of the oviductal isthmus myosalpinx complicating embryo transport suggesting an important role for YAP1 and WWTR1 in structural integrity(10). Beyond what is known in the mouse, YAP and WWTR1 have been independently identified as critical for endometrial stromal cell decidualization. YAP expression increases in the first 48 hours of *in vitro* endometrial stromal cell decidualization and knockdown by shYAP prior to induction of *in vitro* decidualization results in a compromised decidualization response(11). In addition, WWTR1 (formerly known as TAZ), increases during *in vitro* decidualization at day 6 and knockdown of WWTR1 also compromises the expression of decidualization markers IGFBP1 and dPRL (unpublished)(12). These studies have shown roles for YAP and WWTR1 in *in vitro* decidualization but this potential has yet to be explored *in vivo* in the murine uterus. In this study, we generated conditional knockout of YAP and WWTR1 under the *Progesterone receptor Cre* to explore the potential roles and regulation of these Hippo homologs in pregnancy.

Results

Generation of Yap1 and Wwtr1 partial double knockout

Progesterone (Pgr) Cre expressing male mice were crossed to double floxed females ($Yap^{f/f}$ $Wwtr1^{f/f}$) to generate heterozygous founders. Offspring were then backcrossed to generate $Pgr^{Cre/+}$ $Yap^{f/f}$ $Wwtr1^{f/f}$ females for fertility investigation. Resulting mice were genotyped as $Pgr^{Cre/+}$ $Yap^{f/+}$ $Wwtr1^{f/f}$ or $Pgr^{+/+}$ $Yap^{f/f}$ $Wwtr1^{f/f}$ but never as $Pgr^{Cre/+}$ $Yap^{f/f}$ $Wwtr1^{f/f}$. Investigation into the Mouse Genome Informatics database revealed that *Progesterone* and *Yap1* are 0cM apart and therefore it was impossible to generate a full double knockout model utilizing the *Pgr Cre*. Investigation continued into the role of *Yap* and *Wwtr1* in the murine reproductive tract utilizing the partial double knockout model.

Progesterone Cre conditional deletion of Yap1 and Wwtr1 exon 3 does not affect reproductive tract structure

Uteri and ovaries were assessed for recombination of *Yap1* and *Wwtr1* (Figure 1). At 3.5dpc, neither *Yap1* nor *Wwtr1* were differentially expressed in uteri utilizing primers that amplify floxed exon 3, but the target gene *Ccn2* was significantly decreased (Figure 1A-C). However, at 5.5dpc, *Wwtr1* was significantly decreased in pdKO uteri (Figure 1B). Immunohistochemical analysis indicated compartment specific expression of YAP1 and WWTR1 in uteri at 3.5dpc, but expression levels were not significantly different between controls and pdKOs (Figure 1E-F). Evidence of *Yap1* and *Wwtr1* and target gene depletion was not evident in ovaries (Supplementary Figure 1A). In addition, protein expression for both YAP1 and WWTR1 was not differentially expressed in granulosa cells of 3.5dpc ovaries based on immunohistochemistry (Supplementary Figure 1B). In addition to these molecular analyses, no structural differences were

observed in the ovaries, oviducts, and uteri of virgin females at proestrus or at 3.5dpc (Supplementary Figure 2A-B).

Partial ablation of Yap and Wwtr1 induces subfertility

Pgr$^{Cre/+}$ *Yap*$^{fl/+}$ *Wwtr1*$^{fl/fl}$ partial double knockouts (pdKO) produced significantly fewer total pups over the course of a 6-month breeding trial (n=4, Figure 2A). In addition, pdKO females had smaller litter sizes compared to controls (Figure 2B). On average, the pdKO mice bore approximately 50% fewer pups and litters compared to the floxed controls throughout the breeding trial (Supplementary Table 3). In addition, the pdKO mice displayed a reduced capacity to produce pups as time progressed (Figure 2C). In fact, one individual only produced two live born litters when placed with multiple fertile males (Figure 2D). In addition to the subfertility shown throughout the breeding trial, pdKO females in an expanded cohort exhibited significantly reduced first and second litter sizes (Supplementary Figure 3A). This was also associated with increased inter-litter timing (Supplementary Figure 3B). Despite increased inter-litter timing, pdKO body weight measured over an 8-week period matched that of the wild-types (Supplementary Figure 3C). At the termination of the 6-month breeding trial, n=3 per genotype were collected for analyses. These mice did not display any significant differences in body, uterine, nor ovarian weight at the time of collection (not shown) and no alterations in reproductive tract structure were observed grossly nor with histological analyses (Supplementary Figure 2C).

Yap1-Wwtr1 partial double knockout females exhibit decreased decidualization response

Artificial decidualization was maintained for 5 days then uteri collected for analyses. Representative images show unstimulated (left) and stimulated (right) horns for floxed controls and pdKOs (Figure 3A). Uterine wet weight ratio of stimulated to unstimulated horn was not different in the pdKO group compared to controls (Figure 3B). However, mRNA expression of decidualization response genes, *Wnt4* and *Bmp2*, indicated a blunted decidualization response in the stimulated uterine horns of pdKOs compared to controls (Figure 3C).

Loss of Yap1 and Wwtr1 leads to incomplete pregnancy failure

Pregnancy was assessed in control and pdKO mice at various timepoints including implantation (4.5dpc), post-implantation (5.5dpc), early pregnancy (7.5dpc), placentation initiation (9.5dpc), and post-placentation (12.5dpc) (Figure 4). Gross morphology of the uteri was apparently normal at all time points with the exception of 12.5dpc when pdKO mice exhibited many resorption sites (Figure 4A). Quantification of normal implantation sites revealed variance in phenotype. At 4.5dpc, the time of implantation, pdKO females were split with 50% of individuals with positive implantation sites with blue dye injection and 50% of individuals without positive implantation sites (Figure 4B). However, by 5.5dpc the majority of pdKO females had positive implantation sites with numbers comparable to controls (Figure 4B). At 7.5dpc and 9.5dpc, the number of individuals with positive implantation sites decreased to ~40% with ~60% of individuals not having positive implantation sites at 9.5dpc (Figure 4B). At 12.5dpc,

embryonic loss was evident with visually identifiable resorption sites (Figure 4B). In addition, across all timepoints measured, pdKO females exhibited a higher likelihood of being not pregnant compared to controls (33% of individuals, Fisher's exact test $p<0.0001$, Figure 4C).

pdKOs display modest interruptions in embryo transport

Determination of the cause of pregnancy failure prompted investigation into ovulation and fertilization rates and embryo transport. Post-fertilization at 1.5dpc when all ovulated oocytes should be in the oviducts, we noted comparable numbers of unfertilized oocytes (UFO) and 2-cell embryos in pdKOs and controls (Figure 5A). However, at 3.5dpc, the time of embryo entry into the uterus, we noted the emergence of two mutually exclusive groups: pdKO females with embryos found only within the oviducts and pdKO females with embryos found only within the uterus (Figure 5B-C). The total number of visual corpus lutea did not differ between pdKOs and controls and neither did the total number of embryos flushed at 3.5dpc (Figure 5D). In addition, visualization of oviducts indicated appropriate folding patterns (Supplementary Figure 4A)(13). Individual uteri were imaged utilizing tissue clearing to allow visualization of embryos *in situ*. Embryos found within pdKO uteri at 3.5dpc were 50% of the quantity found within control uteri (Figure 5E and Supplementary Figure 4B).

pdKOs exhibit altered maternal endometrial receptivity

To disseminate the cause of delayed embryo entry into the maternal endometrium combined with partially delayed implantation and to rationalize delayed embryonic

development, we investigated endometrial receptivity at 3.5dpc (Figure 6). Expression of progesterone receptor by both mRNA and protein was not altered in pdKO uteri at 3.5dpc (Figure 6A and B). However, we noted significantly decreased target gene expression, *Ihh* and *Nr2f2*, in 3.5dpc uteri (Figure 6A). In addition, luminal epithelial expression of proliferation marker, Ki67, was maintained in pdKO uteri (Figure 6C). Interestingly, estrogen receptor signaling was also decreased at 3.5dpc (Supplementary Figure 5).

pdKO uteri contain embryos exhibiting delayed development

Implantation chamber morphology was notably normal when visualized with whole uterine imaging at 5.5dpc (Figure 7A). However, pdKO uteri contained embryos that morphologically appeared delayed with decreased elongation compared to controls at 5.5dpc (Figure 7B). The majority of embryos visualized (59%) within pdKO uteri were delayed (Figure 7C). Overall, implantation chamber length was not affected despite delayed embryos being found in the majority of implantation sites visualized (Figure 7D). Delayed embryos with decreased elongation morphology had 3D surface volumes significantly lower compared to normal elongated embryos found within both control and pdKO implantation sites (Figure 7E). The ratio of embryo volume to implantation chamber length, however, showed a decrease in those embryos that were identified as delayed (Figure 7F).

pdKOs have a unique transcriptional profile

Whole uterine cross-sections at 7.5dpc from pdKO (n=3) and floxed controls (n=4) were subjected to bulk mRNA sequencing to elucidate the transcriptional repercussions associated with the loss of *Yap1* and *Wwtr1* in the pregnant uterus. Samples separated on an MDS plot based on genotype (Figure 8A). We identified 16,674 total genes after filtering and identified 1,785 differentially expressed genes (DEG) with 884 genes upregulated and 901 downregulated in the knockouts compared to controls (Figure 8B). Differentially expressed genes included a number of genes associated with the Hippo signaling pathway (Figure 8C) and decidualization response genes (Figure 8D). DEG contributed to Gene Ontology Cellular Component terms like extracellular matrix, collagen trimer, collagen-containing extracellular matrix indicating that loss of *Yap1* and *Wwtr1* affected cellular structure (Figure 8E). In addition, upregulated genes were enriched for Rat Genome Database (RGD) disease terms like pre-eclampsia, endometriosis, liver cirrhosis, and pulmonary fibrosis indicating that pdKOs clearly enriched for reproductive diseases associated with pregnancy loss and fibrosis which has classically been associated with Hippo signaling (Figure 8F).

Discussion

We showed that depletion of *Yap1* and *Wwtr1* led to a lack of decidualization response and maternal remodeling. YAP1 and WWTR1 are classically noted to respond to extracellular changes in stiffness transduced through the Hippo signaling pathway and decidualization and pregnancy processes which rely on appropriate extracellular changes to alter the maternal endometrial environment(7). They also classically regulate the transcription of extracellular and structural component genes in addition to

cell cycle regulatory genes(7). It is no surprise that loss of *Yap1/Wwtr1* led to the enrichment of DEG in GO Cellular Component terms like plasma membrane, collagen containing matrix, and extracellular matrix (Supplementary Table 6). Within the upregulated and downregulated DEG of the bulk mRNA sequencing, specific classes of genes included extracellular matrix genes such as collagens, CCNs, laminins, extracellular remodeling genes like matrix metalloproteases (Supplementary Tables 6 and 7). However, differential gene expression analysis of whole tissue makes it difficult to determine whether altered wound healing or fibrosis is occurring in the pdKO females. However, given the phenotypic data that show a progressive loss of fertility in the pdKO females, it is likely that either aberrant wound repair mechanisms or increased scarring and associated fibrosis are occurring. Both wound healing and fibrosis associated markers were found with the DEG at 7.5dpc including the decrease of angiogenic markers *Vegfc*, *Vegfb*, increased *Pdgfrb*, and increased expression of *Il13ra1* and *Il4ra1*. Angiogenesis is associated with wound healing but is negatively associated with fibrosis(14). These results suggest that loss of *Yap1*/*Wwtr1* is leading to decreased wound healing during pregnancy through the downregulation of proangiogenic factors, but that vasculature is responding to a lack of angiogenic signal by upregulating receptor expression on the vascular smooth muscle. In addition, IL13RA1 forms a heteromeric complex with IL4RA and activation of this receptor complex is widely considered pro-fibrotic, supporting that the pdKO uteri may be exhibiting increased fibrosis(14). Supporting this, pathway enrichment for upregulated DEG in Disease RGD included disease terms for fibrotic diseases like pulmonary fibrosis and liver cirrhosis (Supplementary Table). It is likely that loss of *Yap1/Wwtr1*

contributes to both a lack of wound healing and increased fibrosis within the murine uterus during pregnancy and this contributes to the repetitive pregnancy loss seen within the pdKO females.

The deficient uterine receptivity and dysregulation of hormonal signals within the pdKO females is indeed interesting. However, interplay between the Hippo signaling pathway and hormonal response has been observed before. The functional kinases of the Hippo kinase cascade, serine/threonine kinase 3 and 4 (Stk3/4), have been shown to be differentially expressed throughout the murine estrous cycle and indeed primarily under the control of estrogen signaling(15). Indeed, Yap expression is also differentially regulated throughout the murine estrous cycle with its level being highest during estrous and diestrus(8). Importantly, estrus in female mice is when ovulation occurs and 3 days later is when the window of receptivity begins. In addition to the cyclical presence of Yap1 as well as activation of the Hippo signaling pathway, the function of this pathway has also been associated with hormonal action. In particular, in disease states like breast cancer and endometriosis, YAP1 bound to TEAD transcription factors can induce transcription of *ESR1* or alternatively in endometriosis YAP1 can regulate upstream factors that influence *PGR* expression (16, 17). These reports support an indirect method of hormonal control and interpretation of signal, but it is possible within the scope of YAP1/WWTR1 function as transcriptional coactivators that they could play a direct role within hormone receptor function. In one study, YAP/TEAD complexes bound to ESR1 enhancer regions and estrogen response elements (18). We propose that within our model, it is possible that the loss of *Yap1/Wwtr1* and subsequent binding to

TEADs, prevents the acquisition and activation of distal estrogen and progesterone receptor response elements and enhancer recruiters. This would explain why loss of *Yap1/Wwtr1* during the receptive window leads to a failure of Pgr and Esr1 regulated genes to be activated despite appropriate expression of receptor levels during this time (Summary Figure). The mechanistic aspect of this hypothesis remains to be tested but opens a path for novel roles of YAP1/WWTR1 function within the murine uterus.

The incomplete penetrance of phenotype in the pdKO females can be attributed to a lack of recombination of one *Yap1* allele. Both *Progesterone receptor* and *Yap1* are located on chromosome 9 in mice with *Pgr* being located at 8899834-8968612 bp on the sense strand and *Yap1* being located at 7932000-8004597 bp on the antisense strand (Mgi). Both *Pgr* and *Yap1* are located at 2.46cM and due to the basics of recombination efficiency, the likelihood of recombination for these two genes is 0%. Unfortunately, this contributes to the only possible genotype being *Pgr Cre* on the sense strand and one deleted allele of *Yap1* on the antisense strand within any given *Pgr* expressing cell within the murine uterus. The unfortunate proximity of these genes led to the partiality of the double knockout and the lack of complete phenotype. Despite the incomplete penetrance of phenotype, we observed significant differences in pdKO females compared to controls, which compromised fertility. It is likely that complete conditional uterine knockout of *Yap1* combined with *Wwtr1* would lead to a much more severe effect including fully compromised decidualization and fertility due to a lack of maternal remodeling. Currently, we are working to generate cell type specific knockouts to determine the compartmental contributions of total *Yap1* and *Wwtr1* knockout.

Materials and Methods

Animal Models

Pgr$^{Cre/+}$(19) mice were crossed to *Yap*$^{fl/fl}$ *Wwtr1*$^{fl/fl}$(20, 21) to generate *Pgr*$^{Cre/+}$ *Yap*$^{fl/+}$ *Wwtr1*$^{fl/fl}$ partial double knockouts (pdKO). The *Pgr*$^{Cre/+}$ mice are a mixed background of 129Sv × C57BL/6, the *Yap*$^{fl/fl}$ *Wwtr1*$^{fl/fl}$ mice are 129SvEv. Animals were housed and maintained in a designated animal care facility at Michigan State University on a 12-hour light/dark cycle with free access to food and water. All animal procedures were approved by the Institutional Animal Care and Use Committee of Michigan State University.

Fertility Evaluation

Females were co-housed with proven fertile wild-type males for a 6-month breeding trial. Males were rotated in or out of cages if females did not produce a live born litter within one-month from time of set up. For timed mating experiments, proven fertile wild-type males were placed in female cages in the evening. Seminal plugs were checked each morning with day of plug designated at 0.5 days post coitus (dpc). Tail vein injection with Chicago blue dye served as a positive identifier for implantation sites at all time points. Following blue dye injection, female mice were sacrificed for collection at a variety of timepoints including 1.5, 3.5, 4.5, 5.5, 7.5, 9.5, and 12.5dpc. Body weight, uterine wet weight, ovarian wet weight, implantation site number, and gross morphology were catalogued. Uterine, oviductal, and ovarian tissues were divided and flash frozen or stored in RNAlater for downstream RNA and protein analyses or fixed in 4%

paraformaldehyde for histological analysis. A subset of tissues were fixed in 10% DMSO in methanol for tissue clearing and advanced light sheet microscopy.

Artificial Decidualization

Sexually mature (8 weeks or older) female mice were ovariectomized followed by two weeks of rest. Animals were treated with three daily subcutaneous injections of 100ng 17β-estradiol followed by two days of rest then three daily injections of 1mg progesterone plus 6.7ng 17β-estradiol. Six hours following injection on the third day, an intraluminal scratch was performed surgically on the anti-mesometrial side of the endometrium of one uterine horn utilizing a blunted 25G needle. The unscratched uterine horn served as an unstimulated hormonal control. Decidualization reaction was maintained with daily subcutaneous injection of 1mg progesterone plus 6.7ng 17β-estradiol for 5 total days followed by euthanasia (n=5/genotype). Uterine tissues were collected as described above. Decidual reaction was measured by uterine wet weight ratio of stimulated/unstimulated horn and molecular markers *Wnt4*, *Bmp2*, and *Prl3c1* by qPCR of stimulated uterine horn compared to unstimulated horn from the same animal.

Oviductal and Uterine Flushes

Sexually mature female mice (8weeks or older) were mated to proven fertile wild-type males. Oviductal flushes were performed with phosphate buffered saline by inserting a 30G needle into the infundibulum of both oviducts at 1.5dpc (n=6 per genotype). Flushed products were collected, counted, categorized, and imaged. Uterine and

oviductal flushes were performed at 3.5dpc with uterine flushes performed by inserting a 30G needle into the uterotubal junction and flushing toward the cervix utilizing PBS. Flushed products were similarly collected, counted, categorized, and imaged.

Immunohistochemistry

Tissues were fixed in 4% paraformaldehyde, dehydrated in ethanol and xylene, and embedded in paraffin. Sections (6 µm) were deparaffinized and rehydrated in a graded alcohol series followed by antigen retrieval (Vector Laboratories, Burlingame, CA) and hydrogen peroxide treatment. Next, sections were blocked and incubated with antibodies against YAP, WWTR1, ER-alpha, PGR, Ki67, SUSD2 or ASMA overnight at 4◦C (see Supplementary Table 1 for complete antibody information). On the following day, sections were incubated with biotinylated secondary antibodies followed by incubation with horseradish peroxidase conjugated streptavidin. Immunoreactivity was detected using the DAB substrate kit (Vector Laboratories) and visualized as brown staining by light microscopy. Incubation with secondary antibody only served as a negative control. Alternatively, after dehydration, slides were stained with Masson's Trichrome followed by rehydration in a graded ethanol series then cover slipped and visualized by light microscopy. ImageJ image analysis software (NIH, v2.14.0), was utilized to determine a digital HSCORE for staining intensity of luminal epithelium, glandular epithelium, and stromal compartments of each uterine section.

RNA isolation and real-time quantitative PCR

Total RNA was isolated from frozen mouse tissue using TRIzol reagent (Invitrogen, Waltham, MA). About 1 µg of RNA was reverse transcribed to cDNA using a High-Capacity cDNA Reverse Transcription kit according to the manufacturer's instructions (Applied Biosystems, Foster City, CA). Quantitative real-time PCR (qPCR) was performed with SYBR Green PCR Master Mix (Applied Biosystems) using the BioRad CFX Opus 384 qPCR system utilizing primers targeting genes of interest (Supplementary Table 2). Expression was normalized to the average of *36b4* and *18s* per sample and fold change determined compared to time matched floxed controls ($Pgr^{+/+}$ $Yap^{fl/fl}$ $Wwtr1^{fl/fl}$).

RNA-sequencing and data analysis

Total RNA was isolated from flash frozen mouse uteri utilizing TRIzol reagent as described above. Following isolation, RNA was treated with a RNA Clean and Concentrator kit (Zymo) followed by DNAse treatment (TURBO DNA-free kit, Invitrogen) and stored in nuclease-free water at -80°C. Concentration was determined utilizing a Qubit RNA BR Assay Kit (Invitrogen). Samples were sent for RNA integrity analysis then subsequently sent to a sequencing facility for library preparation and sequencing (Michigan State University Genomics Core). Libraries were prepped with Illumina Stranded mRNA Library Prep kit (Illumina) and sequenced (paired end 150bp) on a NovaSeq 6000 Instrument (Illumina) to an average depth of 40 million read pairs per sample. Reads were quality trimmed, adapters were removed using TrimGalore (version 0.6.10), and quality-trimmed reads were assessed with MultiQC (version 1.7). Trimmed reads were mapped to Mus Musculus GRCm39.110 and gene counts quantified using

STAR (version 2.6.0c). Model-based differential expression analysis was performed using edgeR-robust method (version 3.42.4) (22) in R. Genes with low counts per million (CPM) were removed using the filterByExpr function from edgeR. Multidimensional scaling plots, generated with the plotMDS function of edgeR, were used to verify group separation prior to statistical analysis. DEG were identified as FDR P value less than 0.05. Visualization of DEG was performed utilizing EnhancedVolcano (version 1.18.0) to generate a volcano plot. Counts per million of selected DEG were plotted using the box plot function of ggplot2 (version 3.4.4). Gene set enrichment and visualization was completed using the ShinyGO online tool (version 0.80) (23).

Whole-mount immunofluorescence, 3D uterine imaging, and analysis

Uteri were dissected from 3.5 (n=2) and 5.5dpc (n=8) pdKO and control females. Fluorescent staining was performed as previously described(24). Briefly, uteri were subsequently fixed in DMSO:methanol (1:4) then stored at -20°C. Uteri were rehydrated in 1:1, Methanol:PBS + 1% Triton X-100 (PBST) for 15 minutes then washed for 15min in 100% PBST. Tissues were then incubated in a blocking solution of PBS, 1% Triton X-100, and 2% powdered milk for 2 hours at room temperature. Uteri were stained with primary antibodies for E-cadherin (COMPANY), and Cytokeratin 8 (COMPANY) diluted at 1:200 in blocking solution for 5 nights at 4°C. Uteri were then washed in PBS + 1% Triton X six times for 30 minutes each then incubated with fluorescently conjugated Alexa Fluor IgG secondary antibodies at 1:500 (Invitrogen) for 2 nights at 4°C. Uteri were then washed in PBS + 1% Triton X six times for 30 minutes each, dehydrated in methanol then incubated overnight in 3% H2O2 diluted in methanol. Hoechst stain was

utilized to visualize nuclei (COMPANY). Tissues were then washed in 100% methanol twice for 15 minutes each and cleared overnight using BABB (benzyl alcohol:benzyl benzoate, 1:2). Stained uteri were imaged with a Leica TCS SP8 X Confocal Laser Scanning Microscope System (Leica Microsystems) with a white-light laser, using a 10x air objective. For each uterine horn, z-stacks were generated with a 7.0 µm increment, Image analysis was carried out using commercial software Imaris v9.2.1 (Bitplane, Zurich, Switzerland). Embryo location was assessed as described previously(25). Briefly, confocal LIF files were imported into the Surpass mode of Imaris, and Surface module 3D renderings were used to create structures for the oviductal–uterine junctions, embryos and horns. The 3D Cartesian co-ordinates of the center of each surface were identified and stored using the measurement module. The distance between the oviductal–uterine junction and an embryo (OE), the distance between adjacent embryos (EE), and the horn length was calculated using the orthogonal projection onto the XY plane. All distances were normalized to the length of their respective uterine horn. Horns with less than three embryos were excluded from the analysis. These distances were used to map the location of the embryos relative to the length of the uterine horn. The uterine horn was divided into three equally spaced segments—closest to the oviduct, middle and closest to the cervix. These segments were quantified for the percentage of embryos present in each section. Embryos in the oviductal region close to the oviductal–uterine junction were accounted for in the first oviductal segment.

Statistical analysis

Western blot densitometric data were tested for normality then analyzed using a one-way ANOVA with Dunnett multiple comparison correction. qPCR data were tested for normality then log transformed in the case of non-normal data and analyzed by one-way ANOVA. Data that were not normal were analyzed utilizing Kruskal-Wallis nonparametric tests. Statistical analyses were performed utilizing GraphPad Prism 10 (GraphPad Software) and values were considered significant if $p<0.05$.

Data Availability

Raw FASTQ files were deposited in the NCBI Gene Expression Omnibus as GSE.

LIST OF FIGURES AND LEGENDS

Figure 1. YAP1 and WWTR1 expression at 3.5 and 5.5dpc. A. *Yap1* mRNA expression is not significantly different in pdKOs compared to controls in early pregnancy. **B.** *Wwtr1* mRNA expression is significantly decreased in pdKOs at 5.5dpc but not at 3.5dpc compared to controls. **C.** YAP/WWTR1 target gene *Ccn1* is not differentially expressed at 3.5dpc in pdKOs. **D.** *Ccn2*, a YAP/WWTR1 target gene, is significantly decreased at 3.5dpc in pdKOs. **E.** YAP1 protein expression at 3.5dpc and semi-quantitative HSCORE. **F.** WWTR1 protein expression at 3.5dpc and semi-quantitative HSCORE.

Figure 2. pdKOs are subfertile with smaller litter sizes. A. pdKO females had fewer total pups across a 6-month breeding trial. **B.** pdKO females had smaller litter sizes compared to controls across a 6-month breeding trial. **C.** pdKO females exhibited a reduced capacity to produce pups over time. **D.** pdKO females began to lose the ability to bear live born litters after the second litter.

Figure 3. Loss of *Yap1* and *Wwtr1* compromises the decidualization response. A. Representative micrographs of unstimulated (left) and stimulated (right) uterine horns 5 days after artificial decidualization induction. **B.** Uterine wet weight ratio of stimulated over unstimulated horn after 5 days of artificial decidualization. **C.** mRNA fold change of decidualization markers *Wnt4* and *Bmp2* 5 days after artificial decidualization induction.

Figure 4. pdKOs exhibit fetal loss at 12.5dpc. A. Representative micrographs of control (top panel) and pdKO (bottom panel) uteri at various stages of pregnancy. Scale bars = 0.5cm. **B.** Quantification of normal implantation sites across pregnancy in both control and pdKO mice (Mixed-effects model comparison genotype *p*=0.0154). **C.** pdKO females exhibit a higher rate of nonpregnancy compared to controls across all timepoints collected (Fisher's Exact Test, *p*=0.0058).

Figure 5. pdKOs females have delayed uterine embryo entry. A. Quantity of unfertilized oocytes (UFO) and 2-cell embryos flushed from oviducts at 1.5dpc from floxed controls and pdKOs. **B.** Total embryos flushed from oviducts of floxed controls and pdKOs at 3.5dpc. **C.** Total embryos flushed from uteri of floxed controls and pdKOs at 3.5dpc. **D.** Total corpus lutea (CL) and embryos flushed at 3.5dpc. **E.** Representative micrographs of fluorescent imaging of embryos within uteri at 3.5dpc (white=Hoechst, E-cadherin=blue).

Figure 6. *Yap1* and *Wwtr1* are required for appropriate endometrial receptivity. A. mRNA relative fold change of *Pgr* and two target genes *Ihh* and *Nr2f2* at 3.5dpc in whole uteri of controls and pdKOs. **B.** Immunohistochemical staining for PGR and semi-quantitative H-CORE of DAB signal in control and pdKO uteri at 3.5dpc. **C.** Immunohistochemical staining for Ki67 and semiquantitative HSCORE of DAB signal at 3.5dpc in control and pdKO uteri.

Figure 7. Loss of *Yap1* and *Wwtr1* in maternal endometrium induces delayed embryonic development. A. Representative micrographs of whole mount uterine imaging of individual implantation chambers and embryos at 5.5dpc (red=E-cadherin, white=Hoechst, Green=FOXA2). **B.** Representative embryos from controls and pdKOs at 5.5dpc (white=Hoechst, Green=FOXA2). **C.** Quantification of normal and delayed embryos imaged at 5.5dpc. **D.** Plotted implantation chamber length for controls and pdKOs at 5.5dpc. **E.** 3D embryo surface volume of normal and delayed embryos at 5.5dpc. **F.** Ratio of embryo volume to respective implantation chamber length for normal and delayed embryos at 5.5dpc.

Figure 8. Transcriptional changes associated with *Yap1* and *Wwtr1* function during pregnancy. A. MDS plot of all uteri samples sequenced at 7.5dpc for controls and pdKOs. **B.** Volcano plot of all genes identified with significantly differentially expressed genes shown in red. **C.** Log2CPM values of significantly differentially expressed Hippo signaling genes and decidualization associated genes in pdKO uteri compared to controls. **D.** Normalized exon 3 (floxed or excised exon) counts for *Yap1* and *Wwtr1* in control and pdKO uteri. **E.** GO cellular component enrichment for all DEG. **F.** Enrichment of upregulated DEG for Disease RGD terms.

Figure 9. Summary Figure. YAP and WWTR1 are required for Progesterone and Estrogen receptor (PR and ER) signaling during the window of receptivity. Blastocyst attachment is delayed likely due to maintained proliferation in the luminal epithelium. In

addition, loss of YAP1 and WWTR1 in both the endometrial epithelium and stroma leads to suppressed ER and PR signaling compromising pregnancy initiation.

Supplementary Figure 1. Analysis of ovaries from pdKO mice A. mRNA analysis of *Yap1, Wwtr1, Ccn1,* and *Ccn2* of whole ovaries collected at 3.5dpc. **B.** DNA expression of floxed allelles in pdKO and control ovaries at 3.5dpc. **C.** Immunohistochemical analysis of YAP1 and WWTR1 in ovaries at 3.5dpc and semiquantitative HSCORE.

Supplementary Figure 2. pdKO histoarchitechture is comparable to controls in primigravid and multigravida females. A. Representative micrographs of trichrome staining of ovaries, oviducts, and uteri of virgin females at proestrus (8 weeks of age). **B.** Representative trichrome micrographs of ovaries, oviducts, and uteri at 3.5dpc in primigravid females (8-12 weeks of age). **C.** Representative micrographs of trichrome staining of ovaries (left panel), oviducts (center panel), and uteri (right panel) from multigravida breeding trial females (8 months of age).

Supplementary Figure 3. pdKOs exhibit increased inter-litter timing and smaller litter sizes. A. Expanded dataset showing decreased pups per litter in pdKOs compared to controls. **B.** pdKOs exhibit increased inter-litter timing. **C.** pdKOs exhibit a proportional body weight increase to controls over an 8-week period.

Supplementary Figure 4. 3D imaging reveals normal oviductal fold patterning in pdKOs. A. Representative micrographs of fluorescent whole mount imaging of oviducts

of floxed controls (top panel) and pdKOs (bottom panel) at 3.5dpc in primigravid females. Images are whole oviduct (left), longitudinal folds (left middle), transverse folds (right middle), and continuous longitudinal folds (right) (white=Hoechst, blue=E-Cadherin, n=4). **B.** Embryos counted in uterine horns at 3.5dpc with whole mount fluorescent uterine imaging (n=2 females/genotype).

Supplementary Figure 5. Estrogen receptor signaling is not aberrant in pdKOs. A. *Esr1* and target genes, *Muc1, C3, Muc4* mRNA expression in 3.5dpc uteri. **B.** Immunohistochemical analysis of Estrogen receptor expression and semiquantitative HSCORE of positive DAB stain in 3.5dpc uteri.

Table 1. Supplementary Antibodies used for western blot and immunohistochemistry analyses.

Antibody	Company	Serial #	Host Species
YAP1	Cell Signaling Technology	14074	Rabbit
TAZ (WWTR1)	Cell Signaling Technology	72804	Rabbit
ER	Invitrogen	MA5-13304	Mouse
PGR	Invitrogen	MA5-14505	Rabbit
Ki67	BD Pharmigen	BD550609	Mouse
ASMA	Cell Signaling Technology	19245	Rabbit

Supplementary Table 2. Primer sequences.

Gene Symbol	Species	Application	Forward	Reverse

Supplementary Table 3. Breeding trial data.

36b4	Mouse	qPCR	CAT CAC CAC GAA AAT CTC CA	TTG TCA AAC ACC TGC TGG AT
18s	Mouse	qPCR	GTA ACC CGT TGA ACC CCA TT	CCA TCC AAT CGG TAG TAG CG
Wnt4	Mouse	qPCR	AGT GCC AAT ACC AGT TCC G	CAC ACT TCT CCA GTT CTC CAC
Bmp2	Mouse	qPCR	CGC AGC TTC CAT CAC GAA	GCT TCC TGT ATC TGT TCC CG
Ccn1	Mouse	qPCR	CCA GTG TAC AGC AGC CTA AA	CTG GAG CAT CCT GCA TAA GTA A
Areg	Mouse	qPCR	CTG AGG ACA ATG CAG GGT AAA	ATC TGG AAC CAT CCG AAA GC
Prl3c1	Mouse	qPCR	GCC ACA CGA TAT GAC CGG AA	TTT GCT CCC TCC AGA ACG AC
Yap1	Mouse	qPCR	GAA AGG GCT CTA GTG GGT AAA G	AAA TCA GGC TAA GGG AAG TAA GG
Wwtr1	Mouse	qPCR	CCA ATG CAC TGA CCA CTC A	CTC CTC TTG ACG CAT CCT AAT C
Pgr	Mouse	qPCR	TGT CAC TAT GGC GTG CTT AC	CTC CTT CAT CCT CTG CTC ATT T
Esr1	Mouse	qPCR	AAC CGC CCA TGA TCT ATT CTG	AGA TTC AAG TCC CCA AAG CC
Ccn2	Mouse	qPCR	GGG CCT CTT CTG CGA TTT C	ATC CAG GCA AGT GCA TTG GTA
Muc1	Mouse	qPCR	GCT GGT GCT GGT CTG TAT TT	CCA CAG CTG GGT TGG TAT AAG
Muc4	Mouse	qPCR	AAT GTT CCT GCC TAT ACT GCC	TTG TAT GGT TCC TGG GTC AC
Ltf	Mouse	qPCR	ATC TCT GTG CCC TGT GTA TTG	ACA TTT CCT GCC TTC TCA GC
C3	Mouse	qPCR	GTG GTC ACT CAG GGA TCT AAT G	GCT CCA ATC AGG GTG TAG TAA G
Ihh	Mouse	qPCR	CAT CTT CAA GGA CGA GGA GAA C	CGC CAG CAG TCC ATA CTT ATT
Nr2f2	Mouse	qPCR	AGG AGA GAG AGA GAG AGA GAG A	GGA AGC TGA GGG TCA GAT AAA G

Genotype	**n**	**Total number of litters**	**Total number of pups**	**Mean pups per litter**	**Mean litter per mouse**	**Mean pups per litter ± SEM**	**Mean litter per mouse ± SEM**
$Pgr^{+/+}$ $Yap^{fl/f}$ $Wwtr1^{fl/fl}$	4	27	247	9.15	6.75	9.1±0.15	6.75±0.1
$Pgr^{Cre/+}$ $Yap^{fl/+}$ $Wwtr1^{fl/fl}$	4	15	77	5.13	3.75	5.1±0.32*	3.8±0.44*

Supplementary Table 4. Gene Ontology Enrichment for Biological Process for upregulated DEG.

Supplementary Table 5. Gene Ontology Enrichment for Biological Process for downregulated DEG.

Supplementary Table 6. Gene Ontology Enrichment for Cellular Component for upregulated DEG.

Supplementary Table 7. Gene Ontology Enrichment for Cellular Component for downregulated DEG.

Acknowledgements

The authors thank Dr. John Lydon (Baylor College of Medicine) and Dr. Francesco DeMayo (NIEHS) for the *Pgr Cre* mouse model, and Dr. Amy Ralston (MSU) for the *Yap* and *Wwtr1* floxed mouse models. The authors thank and acknowledge that this work was made possible by the excellent technical assistance of Samantha Hrbek, Erin Vegter, and the MSU Vivarium Staff. Research reported in this manuscript is supported by the Eunice Kennedy Shriver National Institute of Child Health & Human Development of the National Institutes of Health under award numbers R01HD099090 to A.T.F., and F31HD107923 to G.E.M. Training for G.E.M. was supported in part by the Eunice Kennedy Shriver National Institute of Child Health & Human Development of the National Institutes of Health under Award Number T32HD087166. Partial support for this work was also provided by MSU AgBio Research, and Michigan State University. This content is solely the responsibility of the authors and does not necessarily represent the official views of the National institutes of Health.

Contributions

GEM, NJ, and ATF conceptualized the study. GEM designed experiments. GEM, NM, EV, and ILPD executed experiments. GEM, NM, and RA performed analyses. GWB, BG, RA, and ATF contributed to intellectual oversight, analytical guidance, and training of GEM. GEM wrote the manuscript. ATF contributed funding for this study. All authors reviewed and accepted the final version of the manuscript.

References

1. Cha J, Sun X, Dey SK. Mechanisms of implantation: strategies for successful pregnancy. Nat Med. 2012;18(12):1754-67. Epub 2012/12/12. doi: 10.1038/nm.3012. PubMed PMID: 23223073; PMCID: PMC6322836.
2. Sternberg AK, Buck VU, Classen-Linke I, Leube RE. How Mechanical Forces Change the Human Endometrium during the Menstrual Cycle in Preparation for Embryo Implantation. Cells. 2021;10(8). Epub 2021/08/28. doi: 10.3390/cells10082008. PubMed PMID: 34440776; PMCID: PMC8391722.
3. Gellersen B, Reimann K, Samalecos A, Aupers S, Bamberger AM. Invasiveness of human endometrial stromal cells is promoted by decidualization and by trophoblast-derived signals. Hum Reprod. 2010;25(4):862-73. Epub 2010/02/02. doi: 10.1093/humrep/dep468. PubMed PMID: 20118488.
4. Ramathal CY, Bagchi IC, Taylor RN, Bagchi MK. Endometrial decidualization: of mice and men. Semin Reprod Med. 2010;28(1):17-26. Epub 2010/01/28. doi: 10.1055/s-0029-1242989. PubMed PMID: 20104425; PMCID: PMC3095443.
5. Gellersen B, Brosens JJ. Cyclic decidualization of the human endometrium in reproductive health and failure. Endocr Rev. 2014;35(6):851-905. Epub 2014/08/21. doi: 10.1210/er.2014-1045. PubMed PMID: 25141152.
6. Meng Z, Moroishi T, Guan KL. Mechanisms of Hippo pathway regulation. Genes Dev. 2016;30(1):1-17. Epub 2016/01/06. doi: 10.1101/gad.274027.115. PubMed PMID: 26728553; PMCID: PMC4701972.
7. Totaro A, Panciera T, Piccolo S. YAP/TAZ upstream signals and downstream responses. Nat Cell Biol. 2018;20(8):888-99. Epub 2018/07/28. doi: 10.1038/s41556-018-0142-z. PubMed PMID: 30050119; PMCID: PMC6186418.
8. Moon S, Lee OH, Kim B, Park J, Hwang S, Lee S, Lee G, Kim H, Song H, Hong K, Cho J, Choi Y. Estrogen Regulates the Expression and Localization of YAP in the Uterus of Mice. Int J Mol Sci. 2022;23(17). Epub 2022/09/10. doi: 10.3390/ijms23179772. PubMed PMID: 36077170; PMCID: PMC9456404.
9. Zhang T, Guo S, Zhou H, Wu Z, Liu J, Qiu C, Deng G. Endometrial extracellular matrix rigidity and IFNtau ensure the establishment of early pregnancy through activation of YAP. Cell Prolif. 2021;54(2):e12976. Epub 2021/01/05. doi: 10.1111/cpr.12976. PubMed PMID: 33393124; PMCID: PMC7849163.
10. Godin P, Tsoi M, Paquet M, Boerboom D. YAP and TAZ are required for the postnatal development and the maintenance of the structural integrity of the oviduct. Reproduction. 2020;160(2):307-18. Epub 2020/06/11. doi: 10.1530/REP-20-0202. PubMed PMID: 32520726.
11. Chen H, Song Y, Yang S, Fu J, Feng X, Huang W. YAP mediates human decidualization of the uterine endometrial stromal cells. Placenta. 2017;53:30-5. Epub 2017/05/11. doi: 10.1016/j.placenta.2017.03.013. PubMed PMID: 28487017.
12. Strakova Z, Reed J, Ihnatovych I. Human transcriptional coactivator with PDZ-binding motif (TAZ) is downregulated during decidualization. Biol Reprod. 2010;82(6):1112-8. Epub 2010/02/19. doi: 10.1095/biolreprod.109.081844. PubMed PMID: 20164440; PMCID: PMC2874497.
13. Harwalkar K, Ford MJ, Teng K, Yamanaka N, Yang B, Burtscher I, Lickert H, Yamanaka Y. Anatomical and cellular heterogeneity in the mouse oviduct-its potential roles in reproduction

666 and preimplantation developmentdagger. Biol Reprod. 2021;104(6):1249-61. Epub 2021/03/12.
667 doi: 10.1093/biolre/ioab043. PubMed PMID: 33693543.
668 14. Wynn TA. Cellular and molecular mechanisms of fibrosis. J Pathol. 2008;214(2):199-210.
669 Epub 2007/12/29. doi: 10.1002/path.2277. PubMed PMID: 18161745; PMCID: PMC2693329.
670 15. Moon S, Lee OH, Lee S, Lee J, Park H, Park M, Chang EM, Park KH, Choi Y. STK3/4
671 Expression Is Regulated in Uterine Endometrial Cells during the Estrous Cycle. Cells. 2019;8(12).
672 Epub 2019/12/19. doi: 10.3390/cells8121643. PubMed PMID: 31847471; PMCID: PMC6952811.
673 16. Ma S, Tang T, Probst G, Konradi A, Jin C, Li F, Gutkind JS, Fu XD, Guan KL. Transcriptional
674 repression of estrogen receptor alpha by YAP reveals the Hippo pathway as therapeutic target
675 for ER(+) breast cancer. Nat Commun. 2022;13(1):1061. Epub 2022/02/27. doi: 10.1038/s41467-
676 022-28691-0. PubMed PMID: 35217640; PMCID: PMC8881512 G.P. and A.K. are Vivace
677 employees. The other authors declare no competing interests.
678 17. Lin SC, Li WN, Lin SC, Hou HT, Tsai YC, Lin TC, Wu MH, Tsai SJ. Targeting YAP1 ameliorates
679 progesterone resistance in endometriosis. Hum Reprod. 2023;38(6):1124-34. Epub 2023/04/18.
680 doi: 10.1093/humrep/dead071. PubMed PMID: 37071897.
681 18. Zhu C, Li L, Zhang Z, Bi M, Wang H, Su W, Hernandez K, Liu P, Chen J, Chen M, Huang TH,
682 Chen L, Liu Z. A Non-canonical Role of YAP/TEAD Is Required for Activation of Estrogen-
683 Regulated Enhancers in Breast Cancer. Mol Cell. 2019;75(4):791-806 e8. Epub 2019/07/16. doi:
684 10.1016/j.molcel.2019.06.010. PubMed PMID: 31303470; PMCID: PMC6707877.
685 19. Soyal SM, Mukherjee A, Lee KY, Li J, Li H, DeMayo FJ, Lydon JP. Cre-mediated
686 recombination in cell lineages that express the progesterone receptor. Genesis. 2005;41(2):58-
687 66. Epub 2005/02/01. doi: 10.1002/gene.20098. PubMed PMID: 15682389.
688 20. Xin M, Kim Y, Sutherland LB, Qi X, McAnally J, Schwartz RJ, Richardson JA, Bassel-Duby R,
689 Olson EN. Regulation of insulin-like growth factor signaling by Yap governs cardiomyocyte
690 proliferation and embryonic heart size. Sci Signal. 2011;4(196):ra70. Epub 2011/10/27. doi:
691 10.1126/scisignal.2002278. PubMed PMID: 22028467; PMCID: PMC3440872.
692 21. Xin M, Kim Y, Sutherland LB, Murakami M, Qi X, McAnally J, Porrello ER, Mahmoud AI,
693 Tan W, Shelton JM, Richardson JA, Sadek HA, Bassel-Duby R, Olson EN. Hippo pathway effector
694 Yap promotes cardiac regeneration. Proc Natl Acad Sci U S A. 2013;110(34):13839-44. Epub
695 2013/08/07. doi: 10.1073/pnas.1313192110. PubMed PMID: 23918388; PMCID: PMC3752208.
696 22. Zhou X, Lindsay H, Robinson MD. Robustly detecting differential expression in RNA
697 sequencing data using observation weights. Nucleic Acids Res. 2014;42(11):e91. Epub
698 2014/04/23. doi: 10.1093/nar/gku310. PubMed PMID: 24753412; PMCID: PMC4066750.
699 23. Ge SX, Jung D, Yao R. ShinyGO: a graphical gene-set enrichment tool for animals and
700 plants. Bioinformatics. 2020;36(8):2628-9. Epub 2019/12/29. doi:
701 10.1093/bioinformatics/btz931. PubMed PMID: 31882993; PMCID: PMC7178415.
702 24. Arora R, Fries A, Oelerich K, Marchuk K, Sabeur K, Giudice LC, Laird DJ. Insights from
703 imaging the implanting embryo and the uterine environment in three dimensions.
704 Development. 2016;143(24):4749-54. Epub 2016/11/12. doi: 10.1242/dev.144386. PubMed
705 PMID: 27836961; PMCID: PMC5201036.
706 25. Flores D, Madhavan M, Wright S, Arora R. Mechanical and signaling mechanisms that
707 guide pre-implantation embryo movement. Development. 2020;147(24). Epub 2020/11/08. doi:
708 10.1242/dev.193490. PubMed PMID: 33158924.
709

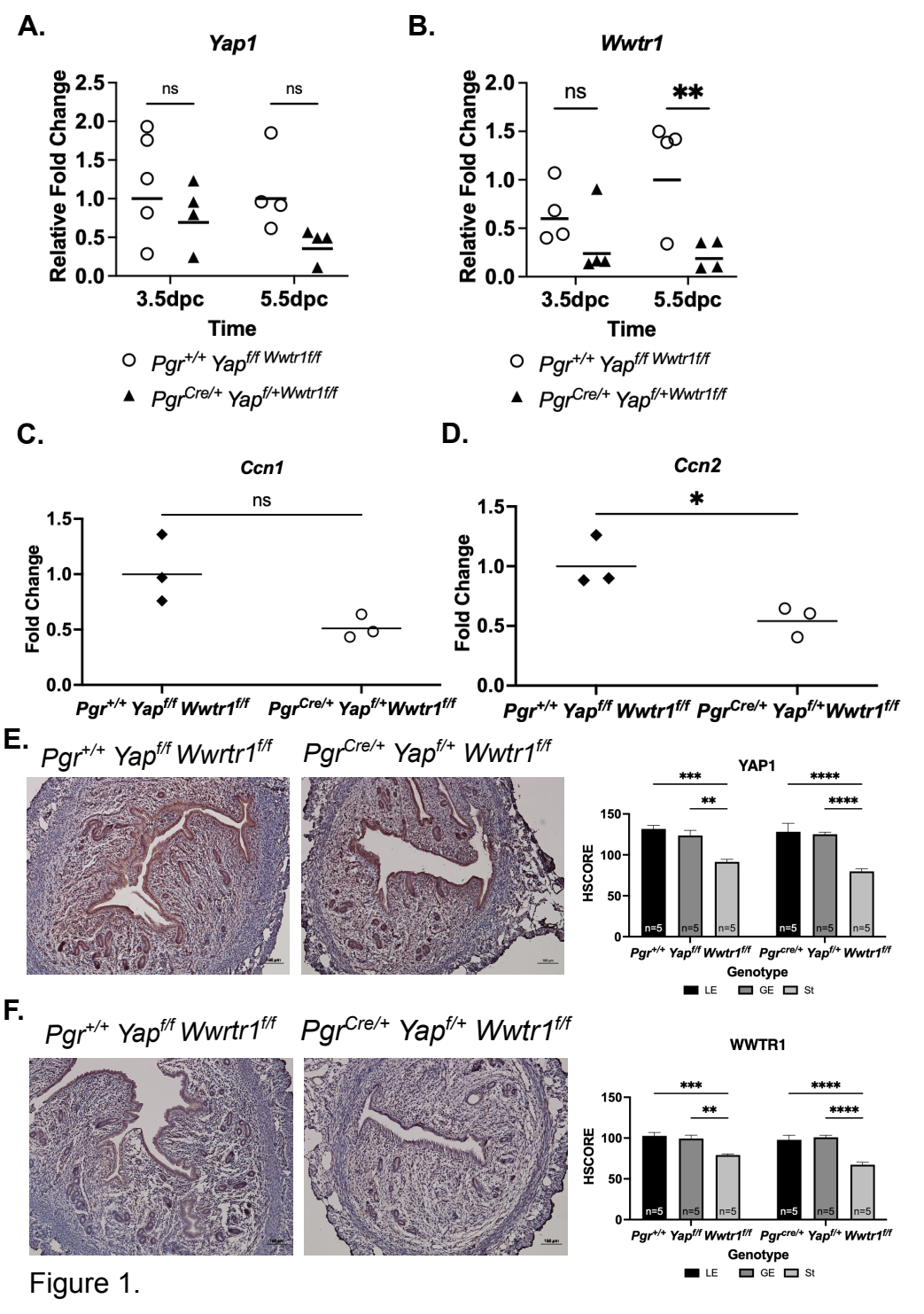
A.
Yap1
Relative Fold Change
2.5
2.0
1.5
1.0
0.5
0.0
ns
ns
3.5dpc
5.5dpc
Time
Pgr+/+ Yapf/f Wwtr1f/f
PgrCre/+ Yapf/+Wwtr1f/f
B.
Wwtr1
Relative Fold Change
2.0
1.5
1.0
0.5
0.0
ns
**
3.5dpc
5.5dpc
Time
Pgr+/+ Yapf/f Wwtr1f/f
PgrCre/+ Yapf/+Wwtr1f/f
C.
Ccn1
Fold Change
1.5
1.0
0.5
0.0
ns
Pgr+/+ Yapf/f Wwtr1f/f
PgrCre/+ Yapf/+Wwtr1f/f
D.
Ccn2
Fold Change
1.5
1.0
0.5
0.0
*
Pgr+/+ Yapf/f Wwtr1f/f
PgrCre/+ Yapf/+Wwtr1f/f
E.
Pgr+/+ Yapf/f Wwrtr1f/f
PgrCre/+ Yapf/+ Wwtr1f/f
YAP1
HSCORE
150
100
50
0
***
**
****
****
n=5
Pgr+/+ Yapf/f Wwtr1f/f
Pgrcre/+ Yapf/+ Wwtr1f/f
Genotype
LE
GE
St
F.
Pgr+/+ Yapf/f Wwrtr1f/f
PgrCre/+ Yapf/+ Wwtr1f/f
WWTR1
HSCORE
150
100
50
0
***
**
****
****
n=5
Pgr+/+ Yapf/f Wwtr1f/f
Pgrcre/+ Yapf/+ Wwtr1f/f
Genotype
LE
GE
St

Figure 1.

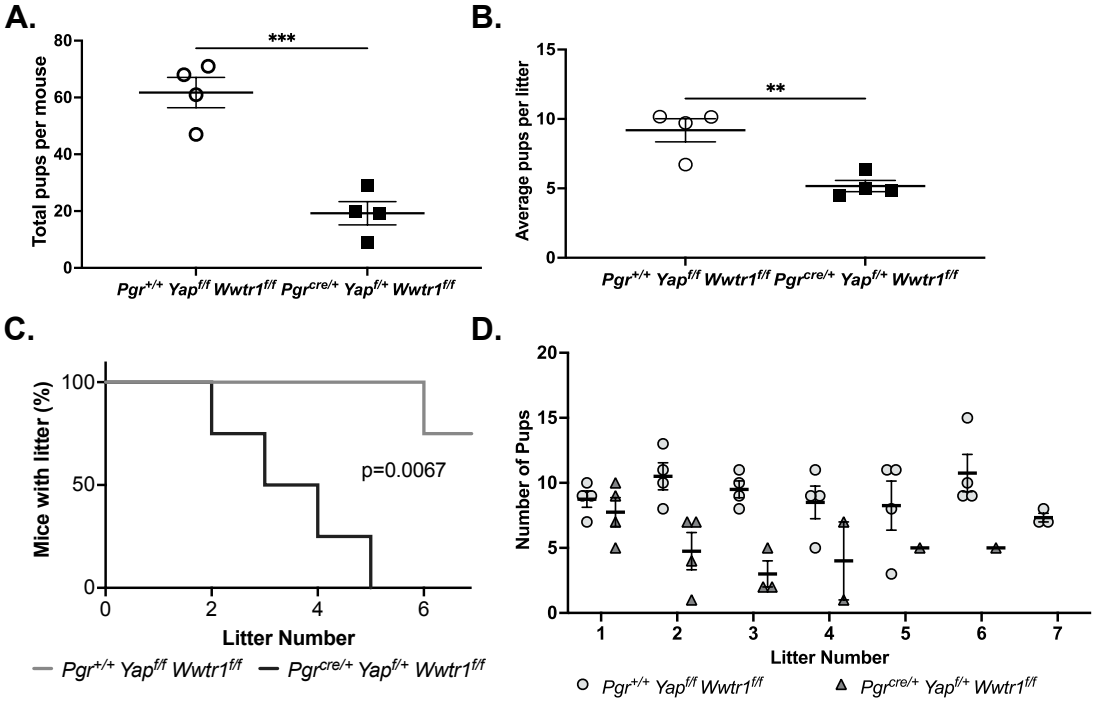
A.
Total pups per mouse
80
60
40
20
0
***
Pgr+/+ Yapf/f Wwtr1f/f
Pgrcre/+ Yapf/+ Wwtr1f/f
B.
Average pups per litter
15
10
5
0
**
Pgr+/+ Yapf/f Wwtr1f/f
Pgrcre/+ Yapf/+ Wwtr1f/f
C.
Mice with litter (%)
100
50
0
p=0.0067
0
2
4
6
Litter Number
Pgr+/+ Yapf/f Wwtr1f/f
Pgrcre/+ Yapf/+ Wwtr1f/f
D.
Number of Pups
20
15
10
5
0
1
2
3
4
5
6
7
Litter Number
Pgr+/+ Yapf/f Wwtr1f/f
Pgrcre/+ Yapf/+ Wwtr1f/f

Figure 2.

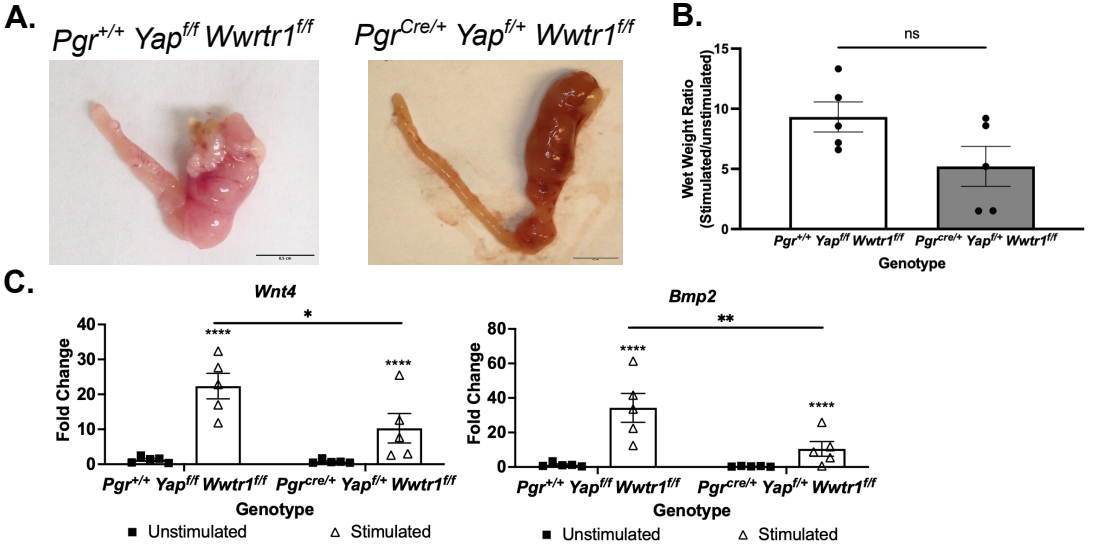
A.
Pgr+/+ Yapf/f Wwrtr1f/f
PgrCre/+ Yapf/+ Wwtr1f/f
B.
ns
Wet Weight Ratio (Stimulated/unstimulated)
15
10
5
0
Pgr+/+ Yapf/f Wwtr1f/f
Pgrcre/+ Yapf/+ Wwtr1f/f
Genotype
C.
Wnt4
*
****
****
Fold Change
40
30
20
10
0
Pgr+/+ Yapf/f Wwtr1f/f
Pgrcre/+ Yapf/+ Wwtr1f/f
Genotype
Unstimulated
Stimulated
Bmp2
**
****
****
Fold Change
80
60
40
20
0
Pgr+/+ Yapf/f Wwtr1f/f
Pgrcre/+ Yapf/+ Wwtr1f/f
Genotype
Unstimulated
Stimulated

Figure 3.

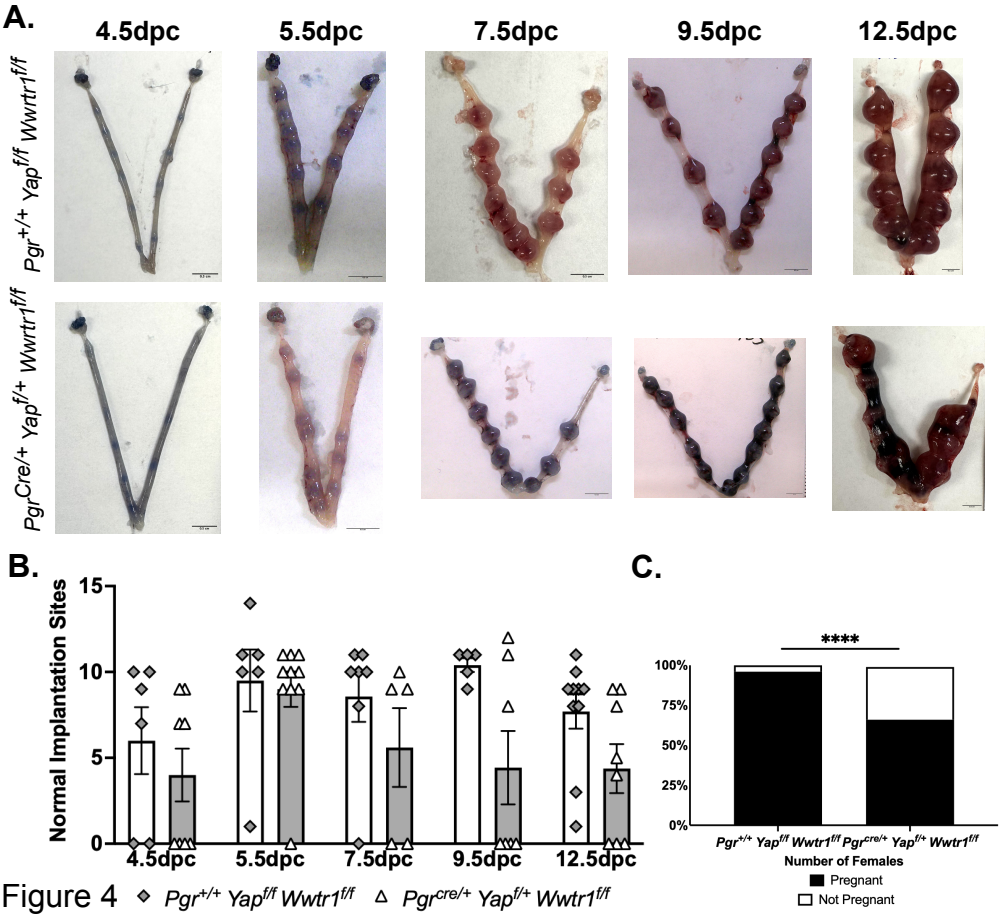

Figure 4 ◆ *Pgr*$^{+/+}$ *Yap*$^{f/f}$ *Wwtr1*$^{f/f}$ △ *Pgr*$^{cre/+}$ *Yap*$^{f/+}$ *Wwtr1*$^{f/f}$

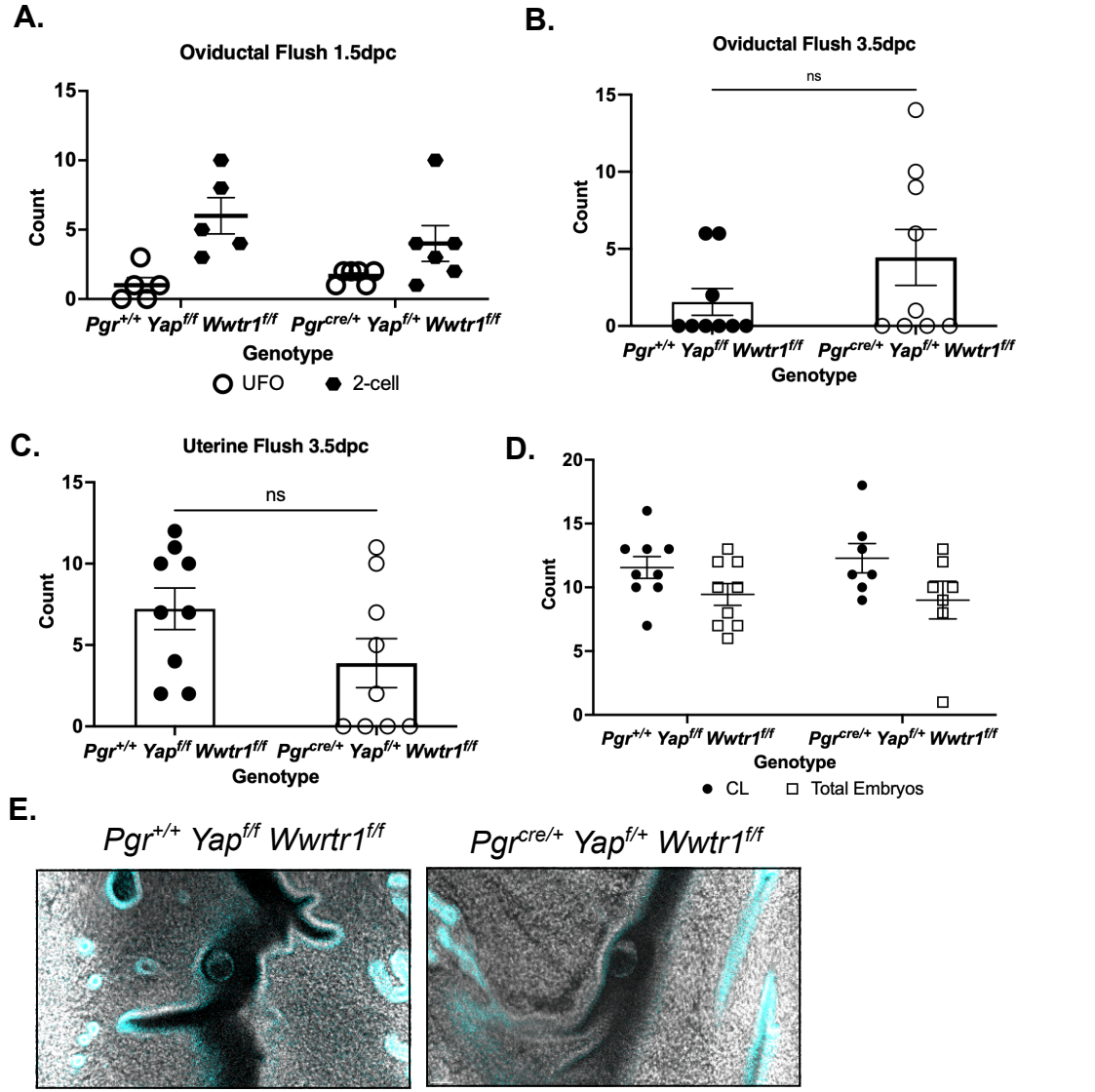
A.
Oviductal Flush 1.5dpc
Count
15
10
5
0
Pgr+/+ Yapf/f Wwtr1f/f
Pgrcre/+ Yapf/+ Wwtr1f/f
Genotype
UFO
2-cell
B.
Oviductal Flush 3.5dpc
ns
Count
15
10
5
0
Pgr+/+ Yapf/f Wwtr1f/f
Pgrcre/+ Yapf/+ Wwtr1f/f
Genotype
C.
Uterine Flush 3.5dpc
ns
Count
15
10
5
0
Pgr+/+ Yapf/f Wwtr1f/f
Pgrcre/+ Yapf/+ Wwtr1f/f
Genotype
D.
Count
20
15
10
5
0
Pgr+/+ Yapf/f Wwtr1f/f
Pgrcre/+ Yapf/+ Wwtr1f/f
Genotype
CL
Total Embryos
E.
Pgr+/+ Yapf/f Wwrtr1f/f
Pgrcre/+ Yapf/+ Wwtr1f/f

Figure 5.

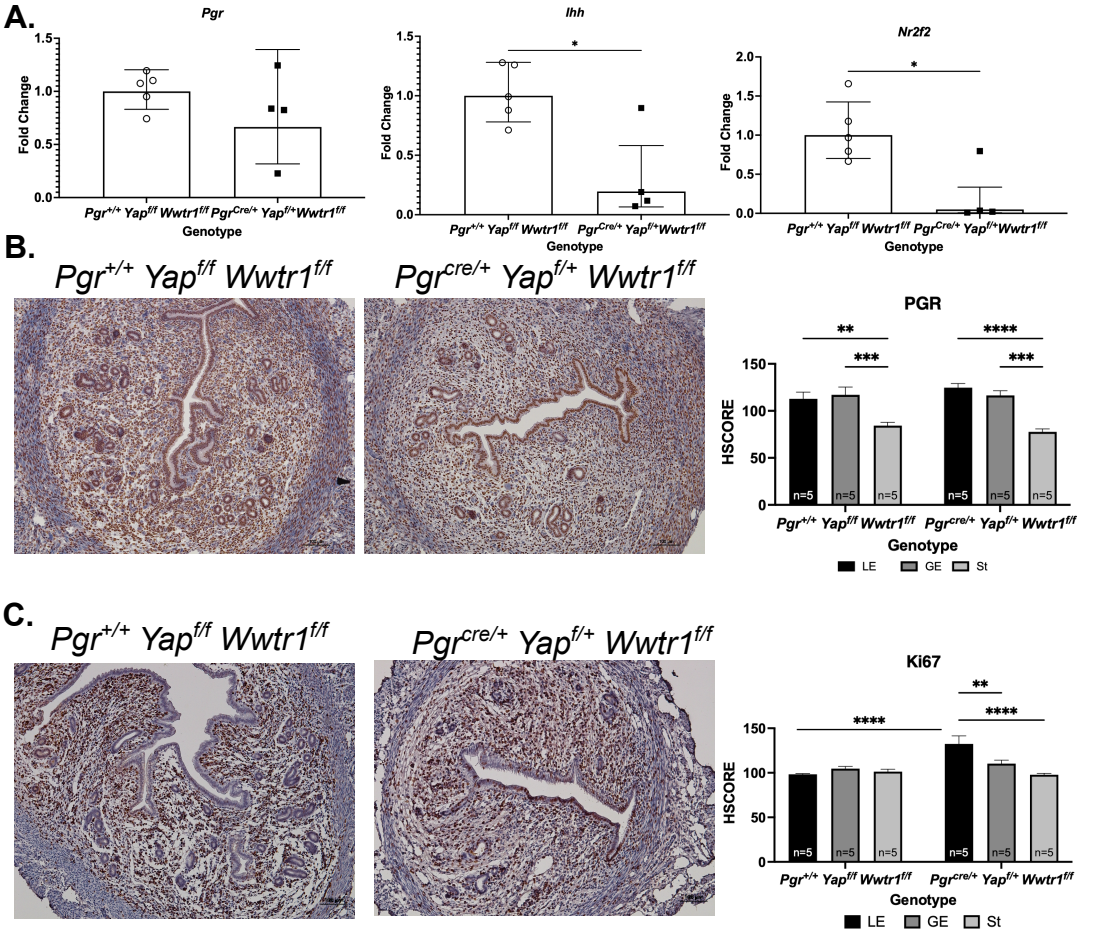
A.
Pgr
Ihh
Nr2f2
Fold Change
Genotype
Pgr+/+ Yapf/f Wwtr1f/f
PgrCre/+ Yapf/+Wwtr1f/f
B.
Pgr+/+ Yapf/f Wwtr1f/f
Pgrcre/+ Yapf/+ Wwtr1f/f
PGR
HSCORE
n=5
LE
GE
St
C.
Pgr+/+ Yapf/f Wwtr1f/f
Pgrcre/+ Yapf/+ Wwtr1f/f
Ki67
HSCORE
Genotype
LE
GE
St

Figure 6.

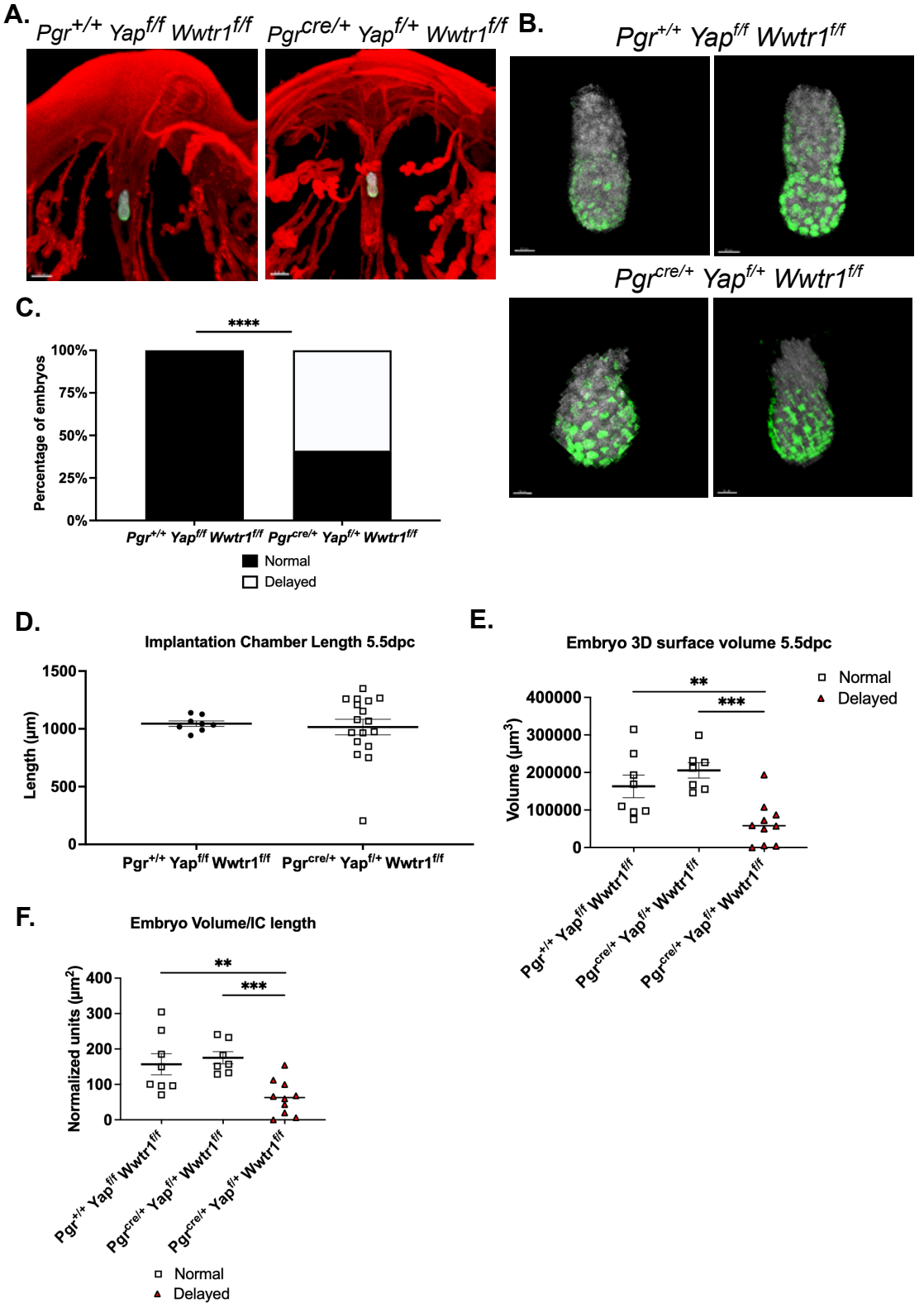
A.
Pgr+/+ Yapf/f Wwtr1f/f
Pgrcre/+ Yapf/+ Wwtr1f/f
B.
Pgr+/+ Yapf/f Wwtr1f/f
Pgrcre/+ Yapf/+ Wwtr1f/f
C.
****
Percentage of embryos
100%
75%
50%
25%
0%
Pgr+/+ Yapf/f Wwtr1f/f
Pgrcre/+ Yapf/+ Wwtr1f/f
Normal
Delayed
D.
Implantation Chamber Length 5.5dpc
Length (µm)
1500
1000
500
0
Pgr+/+ Yapf/f Wwtr1f/f
Pgrcre/+ Yapf/+ Wwtr1f/f
E.
Embryo 3D surface volume 5.5dpc
Normal
Delayed
**
***
Volume (µm3)
400000
300000
200000
100000
0
Pgr+/+ Yapf/f Wwtr1f/f
Pgrcre/+ Yapf/+ Wwtr1f/f
Pgrcre/+ Yapf/+ Wwtr1f/f
F.
Embryo Volume/IC length
**
***
Normalized units (µm2)
400
300
200
100
0
Pgr+/+ Yapf/f Wwtr1f/f
Pgrcre/+ Yapf/+ Wwtr1f/f
Pgrcre/+ Yapf/+ Wwtr1f/f
Normal
Delayed

Figure 7.

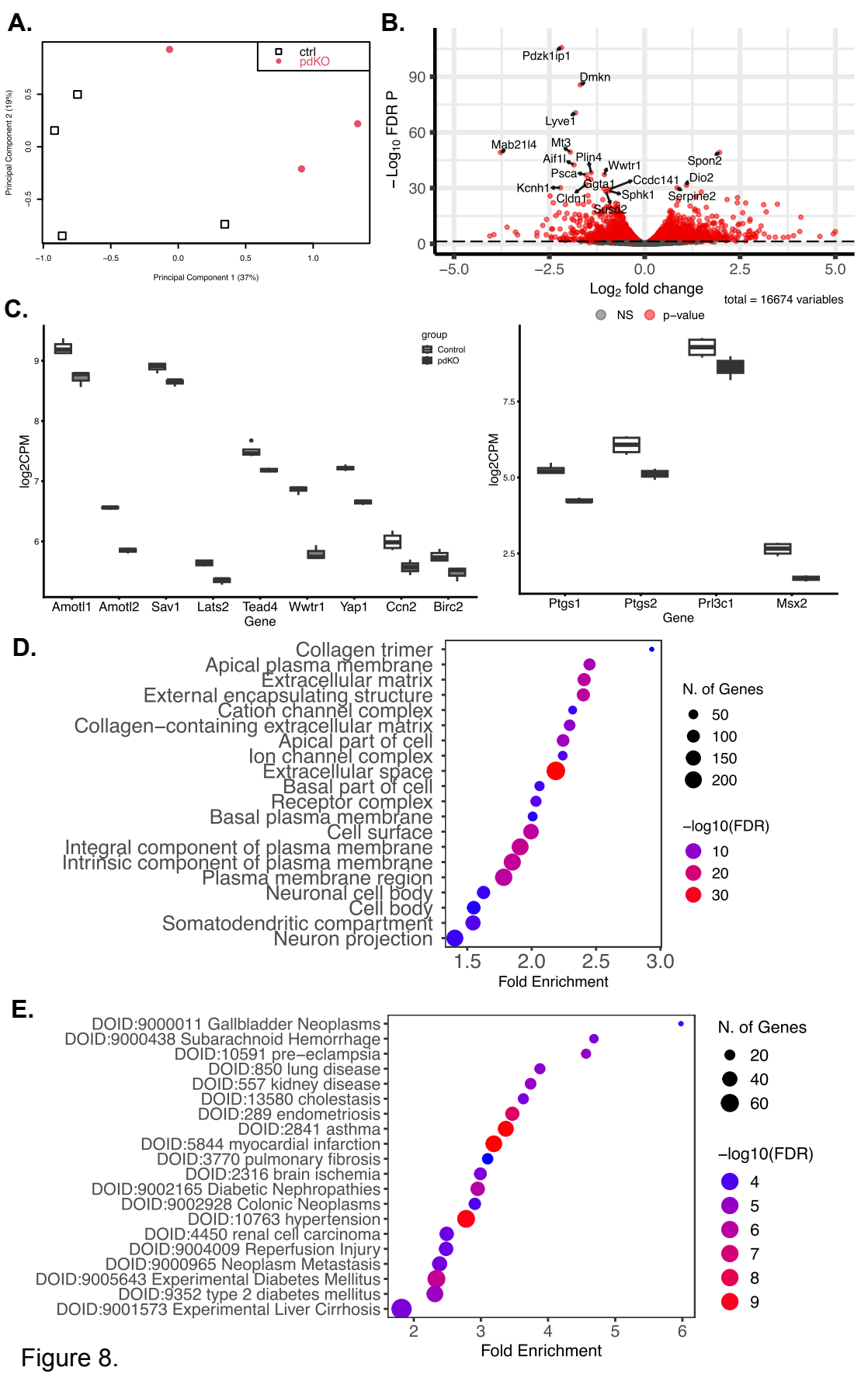
A.
ctrl
pdKO
Principal Component 2 (19%)
Principal Component 1 (37%)
B.
Pdzk1ip1
Dmkn
Lyve1
Mab21l4
Mt3
Aif1l
Plin4
Wwtr1
Spon2
Psca
Ccdc141
Dio2
Kcnh1
Cgta1
Sphk1
Serpine2
Cldn1
Susd2
−Log10 FDR P
Log2 fold change
total = 16674 variables
NS
p−value
C.
group
Control
pdKO
log2CPM
Amotl1
Amotl2
Sav1
Lats2
Tead4
Wwtr1
Yap1
Ccn2
Birc2
Gene
Ptgs1
Ptgs2
Prl3c1
Msx2
D.
Collagen trimer
Apical plasma membrane
Extracellular matrix
External encapsulating structure
Cation channel complex
Collagen−containing extracellular matrix
Apical part of cell
Ion channel complex
Extracellular space
Basal part of cell
Receptor complex
Basal plasma membrane
Cell surface
Integral component of plasma membrane
Intrinsic component of plasma membrane
Plasma membrane region
Neuronal cell body
Cell body
Somatodendritic compartment
Neuron projection
Fold Enrichment
N. of Genes
50
100
150
200
−log10(FDR)
10
20
30
E.
DOID:9000011 Gallbladder Neoplasms
DOID:9000438 Subarachnoid Hemorrhage
DOID:10591 pre−eclampsia
DOID:850 lung disease
DOID:557 kidney disease
DOID:13580 cholestasis
DOID:289 endometriosis
DOID:2841 asthma
DOID:5844 myocardial infarction
DOID:3770 pulmonary fibrosis
DOID:2316 brain ischemia
DOID:9002165 Diabetic Nephropathies
DOID:9002928 Colonic Neoplasms
DOID:10763 hypertension
DOID:4450 renal cell carcinoma
DOID:9004009 Reperfusion Injury
DOID:9000965 Neoplasm Metastasis
DOID:9005643 Experimental Diabetes Mellitus
DOID:9352 type 2 diabetes mellitus
DOID:9001573 Experimental Liver Cirrhosis
Fold Enrichment
N. of Genes
20
40
60
−log10(FDR)
4
5
6
7
8
9

Figure 8.

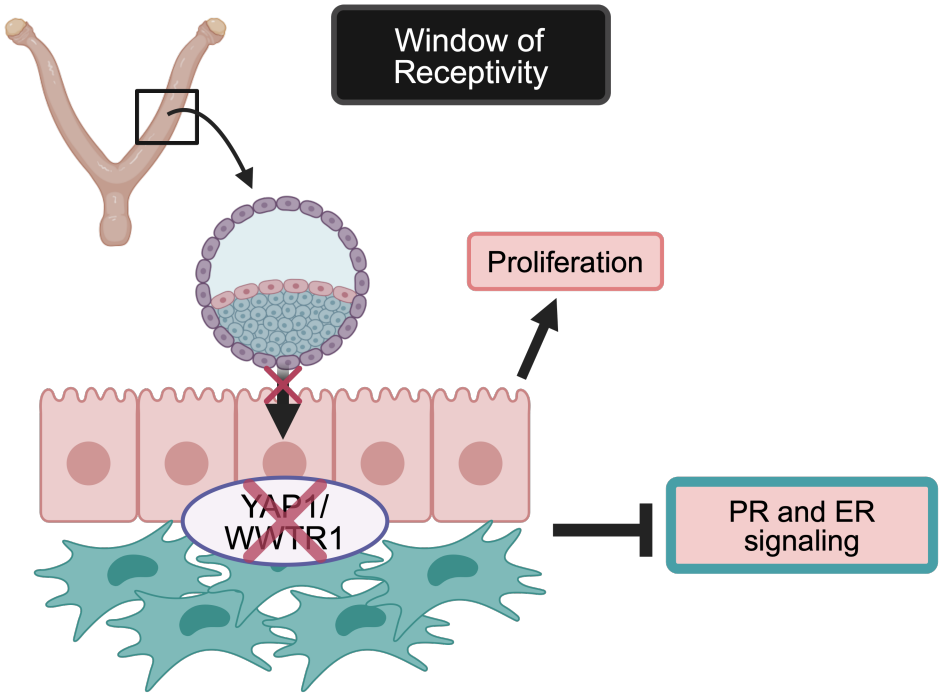
Window of Receptivity
Proliferation
YAP1/ WWTR1
PR and ER signaling

Figure 9.